α-Synuclein Responses: Implications for Early Appearance of Sleep Disorders in Parkinson's Disease

Altair B. Dos Santos
University of Copenhagen: Kobenhavns Universitet
Line K Skanning
University of Copenhagen: Kobenhavns Universitet
Eyd Mikkelsen
University of Copenhagen: Kobenhavns Universitet
Cesar R Romero-Leguizamón
University of Copenhagen: Kobenhavns Universitet
Morten P Kristensen
Academic Services
Anders Bue Klein
University of Copenhagen
Annette Langkilde
University of Copenhagen
Kristi A. Kohlmeier (kak1@sund.ku.dk)
Københavns Universitet https://orcid.org/0000-0003-0183-3816

Short report

Keywords: Neurodegenerative diseases, Prodromal phase, Mechanism of disease, Neuronal alterations

Posted Date: December 28th, 2020

DOI: https://doi.org/10.21203/rs.3.rs-134060/v1

Abstract

Sleep Disorders (SDs) precede motor symptoms of Parkinson's disease (PD), suggesting an early effect of disease processes on sleep control neurons. PD processes involve rises in the protein, α-synuclein, which presents early on in a simple, monomeric form, but later in disease progression, a more complex fibril form appears. We hypothesize that monomeric α-synuclein has deleterious cellular actions on sleep control nuclei. We monitored cellular responses to identified monomeric and fibril α-synuclein in two sleep controlling nuclei, the laterodorsal tegmentum, and the pedunculopontine tegmentum, as well as the substantia nigra, a motor control nucleus which degenerates as a hallmark PD feature. We monitored differential cell death using a fluorescent-based assay following exposure to the simpler form of α-synuclein. In sleep control nuclei, both forms of intrinsic α-synuclein induced excitation, and increased intracellular calcium and the monomeric form heightened putatively excitotoxic, neuronal death, whereas, in the substantia nigra we saw inhibition, decreased intracellular calcium and monomeric α-synuclein was not associated with heightened cell death. These nucleus-specific differential effects suggest previously unappreciated, mechanistic underpinnings of SDs' prodromal PD appearance in PD, and we hypothesize that in the prodromal phase of PD, the early form of α-synuclein compromises sleep-control neurons.

1 Background

Elucidating the neuronal mechanism of non-motor symptoms which precede development of motor disability in Parkinson's disease (PD) offers the hope of earlier disease detection and treatment. Appearance of a sleeping disorder is currently the most specific, and powerful prodromal marker for age-related, α-synucleinopathies such as PD (Postuma et al., 2015; Barber et al., 2017), as these disorders appear up to a decade earlier than motor symptoms. PD movement symptoms are associated with substantia nigra (SN) degeneration and abnormal aggregation of the protein, α-synuclein (α-syn), which changes structure from simple monomers, to more complex aggregates known as oligomers (Bengoa-Vergniory et al., 2017) and, ultimately, to fibrils (Fink, 2006). However, SN degeneration is unlikely to be the cause of the appearance of sleeping disorders (SDs) as they precede the movement impairments of PD. A more likely explanation is that as α-syn levels rise (Wang et al., 2012), α-syn-mediated neurodegeneration starts earlier in sleep and arousal control nuclei than in motor control centers.

The most common SDs in PD encompass activity changes within two state-regulating, pontine brain stem nuclei: the Laterodorsal Tegmental Nucleus (LDT), and Pedunculopontine Tegmental Nucleus (PPT) (Fig. 1A), which, interestingly, are profoundly degenerated in *post mortem* brains of PD patients (Braak et al., 2004; Müller and Bohnen, 2013). Additionally, neurodegeneration in pontine brain stem related to α-syn inclusions has been reported in individuals who were asymptomatic for PD, but diagnosed with REM Sleep Behavior Disorder (Uchiyama et al., 1995; Schenck et al., 1996, Boeve et al., 2007b, a). REM Sleep Behavior disorder is a SD shown to be prodromal to appearance of PD, and believed to involve dysregulation in the pons (Schenck et al., 1996, Boeve et al., 2007a, b). When taken together, we hypothesized that α-syn alters neuronal signaling in the LDT and PPT. Given the appearance of SDs prior

to motor complaints, we further hypothesized that the LDT and PPT exhibit a greater sensitivity to actions of the simpler forms of α-syn than does the SN. To examine these hypotheses, we investigated whether native monomer, as well as fibrillated forms of highly purified α-syn had effects on LDT and PPT neuronal function, calcium dynamics, and whether exposure to α-syn elicited cell death. Further, we compared these effects to those in SN neurons.

2 Materials And Methods

Animals: NMRI mice (Harlan Mice Laboratories, Denmark) aged 12 to 30 days were used under approval in accordance with European Communities Council Directive (86/609/EEC). For calcium imaging analysis in the SN and PPT, after determination that there were no significant sex-based differences in the fluorescence change amplitudes, data from males and females were used (SN: 1 female; PPT: 1 female); whereas, all LDT imaging data sourced from males. The animals were housed with a lactating female under controlled temperature (22–23 °C) and humidity conditions (45–65%) in a 12:12 h light-dark cycle, with water and food available *ad libitum*.

Tissue preparations for electrophysiology and calcium imaging: Following deep anesthesia with inhalation of isoflurane (Baxter A/S, Denmark), a block of the brain containing the LDT, PPT, or SN was excised (Fig. 1A1, 2). The brain block was sectioned into 250 µm slices using a vibratome (Leica VT1200S, Leica Biosystems, Germany) in ice-cold artificial cerebrospinal fluid (ACSF). The standard ACSF contained (in mM) 124 NaCl, 5 KCl, 1.2 $Na_2HPO_4 \cdot 2H_2O$, 2.7 $CaCl_2 \cdot 2H_2O$, 1.2 $MgSO_4$ (anhydrous), 10 dextrose, 26 $NaHCO_3$ at pH 7.4 and an osmolarity of 298–302 mOsm/kg and was saturated with carbogen (95% O_2/5% CO_2).

Recombinant α-syn and size exclusion chromatography (SEC): Human α-syn was recombinantly expressed and purified as previously described (van Maarschalkerweerd et al., 2014) with few modifications. In brief, α-syn was cloned into *E. Coli* BL21DE3 cells using a pET-11a vector construct. Harvested cells were lysed by osmotic shock and non-heat-stable proteins were removed by boiling and centrifugation. α-syn was isolated by ion-exchange chromatography and the monomer was isolated by SEC. Monomer fractions from SEC were pooled and kept in PBS buffer stored at -80 ^{o}C.

Fibrillation assay: α-syn in PBS buffer (1.5–2.2 mg/ml) was fibrillated in a microplate reader (FLUOstar Omega. BMG Labtech) at 37^{o} C with 3 mm sterile glass beads and orbital shaking (700 rpm for 280 s in each 360 s cycle). Samples were aliquoted (150 µl) in a NUNC 96-well optical polymer-based, clear-bottom black plate (Thermo Fisher scientific 265301) and sealed with clear polyolefin tape (Thermo Fisher scientific 232702). Thioflavin T (ThT; 20 µM) was added to three samples, retaining in parallel 3 non-ThT containing samples for the electrophysiology experiments. ThT emission was recorded at 480 ± 10 nm upon excitation at 450 ± 10 nm. Fibril samples were collected after 7 days, to ensure full fibril maturation, and thereafter stored at room temperature. ThT fluorescence for the 7 day fibrillation assay are shown in Fig. 1B1 as the mean of a triplicate run, with insert detailing the first 24 h.

Circular Dichroism (CD): The secondary structure of α-syn samples was investigated to confirm monomeric and fibrillar states. CD was measured on monomer and fibrillated α-syn samples, respectively, using a JASCO J-1500 CD spectrometer. Samples were diluted to a final concentration and placed in a cuvette with a light path of 1 mm. Spectra were collected from 260 – 190 nm, with a bandwidth of 1 nm, scanning speed of 100 nm/min, and a temperature of 25^{o} C. The final specters were made as accumulations of three. In Fig. 1B2, CD spectra of the secondary structure of monomeric and fibrillated α-syn (0.15 mg/ml) are shown indicating random coiling of monomeric α-syn, consistent with the native, intrinsically disordered form, and β-sheet structure after fibrillation.

α-syn, lysozyme, AMPA preparation and application: The highly purified monomeric form of α-syn was stored in solution at -80^{o} C in aliquots of 10 µl (150 µM) until use. Aliquots (150 µM) of α-syn fibrils were kept at room temperature and used within a maximum of 2 weeks. In initial experiments we found that 70 nM of α-syn induced a short-duration, membrane response; whereas, in the same cell, 100 nM induced a longer-lived shift in current amplitude, therefore, we decided to continue with 100 nM, which had been used in other studies (See Supplementary Fig. 1). The final concentration of α-syn diluted in ACSF was applied for 3–4 min after the establishment of baseline conditions. As lysozyme exhibits a similar molecular weight as α-syn (14 kDa), it aggregates and forms fibrils in solution, and it has been extensively utilized as a control for non-specific peptide effects in α-syn studies (Buell et al., 2011; Coelho-Cerqueira et al., 2013), we evaluated whether lysozyme elicited membrane actions to control for non-specific peptide effects. Lysozyme solution (1 mM) was stored at 5^{o} C in aliquots of 2000 µl until use and was diluted in ACSF to a final concentration of 100 nM and applied for 3–4 min via the slice bath, which failed to elicit an excitatory response in LDT neurons (n = 3; Fig. 1C4). Repeatable effects of α-syn in individual neurons indicated that membrane effects were not due to acute excitotoxicity (n = 3; data not shown). Recovery to baseline and rises in calcium induced by a subsequent application of 1 µM AMPA (α-amino-3-hydroxy-5-methylisoxazole-4-propionic acid; 3 ml) confirmed that changes in calcium by α-syn were not due to acute cell death (n = 5; data not shown).

Patch clamp recordings: Borosilicate glass patch pipette electrodes were fabricated using a horizontal puller (P-97, Sutter Instruments, USA), and filled with an intracellular solution containing in mM: 144 K-gluconate; 2 KCl; 10 HEPES; 0.2 EGTA; 5 Mg-ATP and 0.3 Na-GTP, with a resulting pipette resistance of 6–11 MΩ. The brain slice was placed in the recording chamber and 1.2 ml/min of carbogenated ACSF was continuously perfused. Cells were visualized with a 60 x water immersion objective coupled to an upright microscope (BX50WI, Olympus; Japan) with an infrared Dodt gradient contrast system (IR-DGC; Luigs & Neumann, Germany) and a CCD camera (CCD-300ETRC; DAGE-MTI, Michigan City, IN). A patch clamp EPC9 amplifier (HEKA, Germany) and the software Pulse (HEKA; version 13.0) were used in voltage clamp mode and the holding voltage was maintained at -60 mV. Following membrane breakthrough, and at least a 7 min stabilization period, data were collected. Recordings of membrane currents were sampled at a rate of 1 kHz using AxoScope 10.2, and an Axon miniDigi 1B digitizer (Molecular Devices Corporation, USA). Combined patch clamp recordings and calcium imaging were conducted with a different setup in voltage clamp mode with a EPC9 amplifier guided by Pulse (version 9.0); and, membrane current

recordings were sampled at 10 kHz using AxoScope 10.2 (Molecular Devices Corporation, USA) and an Axon Digidata 1440A digitizer (Molecular Devices Corporation, USA).

Identification of cell Phenotype: For *post hoc* identification of the recorded cells as being present within the perimeter of the cholinergic LDT and PPT, or to phenotypically-identify recorded neurons, in some recordings, Alexa-594 was included in the intracellular solution, and immunohistochemistry for brain-derived nitric oxide synthase (bNOS), which is a validated marker of cholinergic neurons in the mouse LDT and PPT, was performed (Veleanu et al., 2016). After the recording, slices were submerged in 4% paraformaldehyde and stored overnight. Slices were then cryoprotected by saturation in a 30% sucrose solution and resectioned. Immunohistochemical labeling for bNOS was conducted following previously reported protocols on the resectioned tissue (Veleanu et al., 2016). Figure 1E shows representative examples of cells recorded in this study (Alexa-594-positive), which were identified as cholinergic or non-cholinergic based on presence or absence of bNOS. In order to evaluate the phenotype of neurons in the SN, we evaluated firing frequency, degree of presence of an I_h current, and spike cessation during electrophysiological recordings in current clamp recording mode (Fig. 1F) (Blythe et al., 2009). To evaluate firing frequency, current was applied which depolarized putative dopamine-containing neurons sufficiently (-50 mV to -45 mV) to induce a regular, slow firing of action potentials (< 4–5 Hz). To determine presence of I_h a large hyperpolarizing pulse (-150 pA; 1–2 sec duration) was used to evaluate appearance of a prominent 'sag' which is a shift in the voltage of the membrane back towards a more depolarized potential. To evaluate blockade of action potential firing, a large amplitude depolarizing current step (+ 150 pA; 1–2 sec duration) was applied and cessation of action potentials was monitored.

Multiple cell and single cell calcium imaging: Single-photon calcium imaging based on the ratiometric fluorescent calcium indicator dye (excitation wavelengths 340 and 380 nM), fura-2 acetoxymethyl ester (fura-2 AM) was conducted. Dye loading of brain slices was performed as in previous studies (Ipsen et al., 2018). For single-cell calcium imaging, bis-Fura 2 (25 μM, Molecular Probes) replaced EGTA in the intracellular pipette solution. For both single and multiple cell calcium imaging, changes in fluorescence emitted within selected regions of interest encompassing cells were detected using a cooled CCD fluorescence camera system (12-bit Sensicam, PCO Imaging, Germany) controlled by the imaging software Live Acquisition (TILL Photonics, Germany).

Neurotoxicity assay: Coronal slices containing LDT or SN were incubated for a period of 7½ hours in α-syn_M (100 nM) or in control solution under the same time protocols and carbogen (95% O_2/5% CO_2) was continuously supplied. Another investigator who was blinded to slice treatment conducted the identification of cell viability (C.R.R.L). The slices were incubated for 3 periods of 5 minutes in 1 μg/ml solution of both propidium iodide (PI; Sigma-Aldrich) to identify dead cells and DAPI which stains live cells (Sigma-Aldrich) with a pH of 7.4. Fluorescent signals were detected by an upright Zeiss microscope (Zeiss 59 fluorescent filter cube sets, wavelengths PI: 472–578 nm; DAPI: 358–463 nm) coupled to a monochrome CCD camera (Axiocam MRM, Zeiss, Germany) controlled by Axioskop 2 software (AxioVision 4.6, Zeiss). ImageJ software (National Institutes of Health, Bethesda, MD) was used to

analyze the collected images and count the number of DAPI and PI-labeled cells. The total cell count was calculated as PI-positive plus DAPI-positive cells.

To compare relative presence of bNOS-positive cells in the LDT, coronal LDT slices were bisected and one half was incubated in control solution, and the other half in one of two α-syn$_M$ containing solutions (200 nM or 500 nM) for 7 h. Following immunohistochemical procedures, cells were determined to be cholinergic based on presence of bNOS. All bNOS-positive cells within the border of the LDT were counted, and for presentation in paired plots, the numbers of positive cells in the α-syn$_M$ -exposed hemi-slice were normalized to control which was the other half of the same slice.

Real-time cell viability: Slices containing the LDT were bisected, individual cells were visualized and patch clamp and calcium imaging recordings were initiated in the same cell. α-syn$_M$ (500 nM) was bath applied, and after filling the recording chamber, perfusion was halted to ensure continuous exposure to α-syn. As a control, the same protocols were conducted on the other half of the slice with the exception of application of peptide. After completing the calcium imaging recording, PI was added to the recording chamber (2 µl; 0.1 µg/ml), and real-time increases in fluorescent signal of PI were measured by time-lapse imaging using the excitation wavelength of 545 nm and the appropriate filter set (Chroma, USA).

Data analysis and statistics: Calcium imaging data were analyzed in Igor Pro 6 (Wavemetrics, USA). Response amplitude and polarity were quantified with changes in fluorescence below 4% considered too small to reliably discern from background noise. The ratiometric measures of changes in fluorescence are shown in graphs as %DF/F. DF/F is the difference between the average of a series of data points at the maximum change in fluorescence following drug application and the average baseline fluorescence (F) relative to F, with ascendant deflection indicating intracellular calcium elevation. Amplitudes of membrane currents were measured (the difference between baseline and maximum deflection) by using AxoScope 10.5 (Molecular Devices, USA). In Figs. 1 and 2, the axis label, *Response Frequency* equals the percentage of tested cells which responded with membrane current or changes in calcium, and the axis label, *Evoked Polarity* indicates the polarity (inward or outward) of the current or increase or decrease in calcium elicited in the population of responding cells, respectively. Statistical analyses of data were performed in Prism (version 7.0, GraphPad, USA). Results are presented as mean values ± SEM with the degrees of freedom (df). The figures were prepared using Igor Pro software, Graphpad Prism and Matlab R2018b. The n reported reflects numbers of single neurons recorded and represents neurons collected from at least 3 different animals which sourced from different litters. Sample sizes were determined from past experiences with electrophysiological recordings in order to limit unnecessary loss of animal life in adherence to 3R guidelines. Differences in numerical data were tested using a one-way ANOVA with Tukey's posthoc test, or a two-way, Paired or Unpaired Student's t-test, and reporting of the *f* or *t* statistic is included as per APA style guidelines. Differences in categorical data were examined using the Fisher's exact test, two-way Chi Square test, or a three-way Chi Square test that in cases of overall significance, was followed by a *post hoc* Fisher's exact test to identify which contingency table cells differed significantly from expected outcomes. The alpha level for statistical significance was set at 0.05, and the exact *p* value is presented.

3 Results

α-syn fibrillation and characterization

α-syn monomer fractions were frozen in solution directly from size exclusion chromatography to avoid aggregate formation. A Thioflavin T (ThT) assay was used to monitor the fibrillation of α-syn, and displayed a typical sigmoidal curve indicating fibril formation (Fig. 1B1). The secondary structure of α-syn was investigated with circular dichroism (CD) showing the expected random coil for monomeric α-syn and β-sheet structure for the fibril form (Fig. 1B2).

Membrane Responses

The monomeric and fibril forms of α-syn induced membrane currents in the majority of LDT, PPT and SN neurons. Surprisingly, the polarity of the elicited currents was opposite in the sleep-regulating LDT and PPT to those elicited in the motor-controlling SN. Inward currents were induced in the sleep-regulating nuclei, whereas, outward currents were elicited in SN neurons (Fig. 1C). The proportion of LDT neurons responding to monomeric α-syn (100 nM) was greater than the proportion of SN neurons responding to this simple form of the protein (LDT: n = 35/35 and PPT: n = 8/8 vs. SN: n = 6/11; Fisher's test; df:1, p = 0.0003; df:1, p = 0.04, respectively). The more complex, fibril form of α-syn produced a significantly higher response rate in the SN than the monomeric form (Percentage Responding: Monomer: 54.5%, n = 6/11; Fibril: 100%, n = 7/7, Chi Square, df: 1, p = 0.0358), and the amplitudes of the currents were significantly greater (Monomer: 15.1 ± 3.9 pA, n = 6; Fibril: 33.7 ± 4.1 pA, n = 7; Unpaired Student's t-test, $t(11) = 3.18$, p = 0.008; Fig. 1D). Within the LDT and PPT, the proportions of cells responding to, and the amplitudes of inward current induced by α-syn were not significantly different for the two forms of the protein (Fibril LDT: n = 7; PPT: n = 8; Unpaired Student's t-test, $t(40) = 0.81$, p = 0.7; t (14): 0.58, p = 0.5, respectively).

Calcium Responses

α-syn altered the concentration of intracellular calcium in the majority of cells examined. Monomeric α-syn induced responses in most calcium indicator-labeled cells in the LDT (n = 56/68) and PPT (n = 45/54) (Fig. 2A). While the fibril form elicited calcium changes in even larger proportions of cells, this difference was not significant (LDT: n = 60/62, PPT: n = 56/60, Fisher's test, df: 1, p = 0.2). Among responding LDT and PPT cells, the majority of changes in fluorescence induced by either form of α-syn indicated calcium increases (Monomeric: LDT: n = 38/56; PPT: n = 30/45; Fibril: LDT: n = 43/60; PPT: n = 34/56; Fig. 2A). Monomeric α-syn elicited calcium responses in a significantly lower proportion of cells in the SN (n = 24/41) than in LDT or PPT (Fisher's test, df: 1, p = 0.008; df: 1, p = 0.01). Further, a relatively higher proportion of cells in SN exhibited calcium decreases (SN: n = 16/24) than in LDT or PPT (Fisher's test, df: 1, p = 0.01; df: 1; p = 0.04; Fig. 2A).

Neurotoxicity assays

As we hypothesized that continuous exposure to early forms of α-syn could have adverse effects on sleep control but not motor control neurons, we examined neuronal death induced by relatively brief, but

continuous exposure to α-syn. Accordingly, LDT and SN slices were incubated in monomeric α-syn (100 nM) or control solution for 7 ½ hours and cell viability fractions were calculated as the ratio of living cells (DAPI-positive) to the total number of cells (DAPI-positive + PI-positive). Relative to control slices, α-syn-exposed LDT slices exhibited a greater proportion of dead cells (Control: n = 4; α-syn: n = 7; Unpaired Student's t-test, $t(9) = 2.52$, $p = 0.03$; Fig. 2B) and fewer surviving cholinergic cells (Fig. 2C). However, SN slices showed no indication of heightened cell death over control (Control: n = 8; α-syn: n = 7; Unpaired Student's t-test, $t(13) = 0.04$, $p = 0.96$, Fig. 2B).

Single cell recordings of membrane effect, calcium influx and real-time, cell viability assay

As we observed effects on membrane currents, calcium levels, as well as heightened cell death by monomeric α-syn in separate populations of cells in sleep control nuclei, we next examined whether those effects co-occurred in the same cell. Thus, in LDT slices exposed to a high concentration of monomeric α-syn (500 nM), we tracked neuronal viability in real-time using PI fluorescence and, within the same neuron, we monitored the membrane current and intracellular calcium response. As control, the same protocols were conducted in the other half of the slice, which was not exposed to α-syn. In all neurons tested, α-syn induced inward currents (-140.5 ± 11.3 pA, n = 4), and an increase in intracellular calcium levels (39.7 ± 10.7% DF/F, n = 4), which were significantly different from control conditions (Fig. 3A, B, C). Subsequent real-time recordings of PI fluorescence showed a significantly shorter lifetime of the cells which were α-syn-exposed compared to control cells (α-syn: 93.7 ± 14.3 min; n = 4, control: 163.3 ± 29.6 min, n = 3, Unpaired Student's t-test; $t(5) = 2.3$; $p = 0.04$; Fig. 3C3).

4 Conclusions

The most common SDs PD patients experience prior to the disease-defining motor symptoms are REM Sleep Behavior Disorder and Excessive Daytime Sleepiness (Schenck and Mahowald, 2002; Abbott et al., 2005; Leng et al., 2018; Postuma et al., 2019). The LDT and PPT play a role in both of these SDs (Van Dort et al., 2015; Kroeger et al., 2017; Boucetta et al., 2014). Within the LDT and PPT, in addition to excitatory currents, monomeric α-syn induced intracellular calcium increases, which could trigger calcium-dependent apoptotic processes of cell death. This conclusion is supported by our findings of cell death promotion in the LDT by even relatively brief exposure to an early-appearing form of α-syn, which does not induce damaging effects in a motor control nucleus in our study, and in other studies (Angelova et al., 2016).

(*Relevance to SN, see Supplemental Material*).

Using multiple, naturally-occurring isoforms of α-syn, which were carefully prepared and validated, our study is the first to report membrane effects of pure monomeric and confirmed fibril forms of α-syn in native, mammalian neurons when extracellularly applied; moreover, our findings indicate the toxic potential of the monomeric form of this protein. Furthermore, our data document a functional difference in cellular responses to α-syn between LDT, PPT and SN neurons, thusly providing the first data for a mechanistic explanation regarding why SDs precede motor symptoms in PD. These results should open

the path to investigations leading to a deeper understanding of the cellular mechanisms underlying α-syn effects resulting in non-motor symptoms of PD, which could serve as targets for earlier disease intervention.

5 List Of Abbreviations

Sleep Disorders – **SDs**; Parkinson's disease – **PD**; Substantia Nigra – **SN**; α-synuclein - **α-syn**; Laterodorsal Tegmental Nucleus – **LDT**; Pedunculopontine Tegmental Nucleus – **PPT**; Rapid Eye Movement - **REM**; Naval Medical Research Institute - **NMRI**; Size Exclusion Chromatography – **SEC**; Thioflavin T – **ThT**; Circular Dichroism – **CD**; α-amino-3-hydroxy-5-methylisoxazole-4-propionic acid – **AMPA**; Brain-derived Nitric Oxide Synthase –**bNOS**; Fura-2 Acetoxymethyl Ester - **Fura-2 AM**; Propidium Iodide – **PI**; 4',6-diamidino-2-phenylindole - **DAPI**; Fluorescence – **F**; Lysozyme – **Lyz.**

6 Declarations

Ethics approval and consent to participate:

animals were used under approval in accordance with European Communities Council Directive (86/609/EEC)

Consent for publication:

Non applicable

Availability of data and material:

data are available from the corresponding author on reasonable request

Competing interests:

All authors declare that there are no conflicts of interest in regard to this manuscript.

Funding:

Coordenação de Aperfeiçoamento de Pessoal de Nível Superior (CAPES), Brazil; Lundbeck Foundation Initiative BRAINSTRUC (2015-2666).

This research was funded by Coordenação de Aperfeiçoamento de Pessoal de Nível Superior (CAPES), Brazil in the form of PhD Grant to Altair Brito dos Santos. Line K. Skaanning and Annette E. Langkilde received financial support for the resources used in this study from the Lundbeck Foundation Initiative BRAINSTRUC (2015-2666, Denmark). None of the funders had any control over study design. No other funding was received for the work presented in this report.

Authors' contributions:

A.B.D.S., A.B.K., M.P.K. and K.A.K. initiated the study and designed the experimental strategy. L.K.S. and A.E.L. expressed and characterized protein structure. A.B.D.S. and E.M. performed and analyzed electrophysiological, and calcium imaging experiments. A.B.D.S and C.R.R.L performed neurodegeneration imaging experiments and data analyzes A.B.D.S. and K.A.K. performed statistical evaluations. L.K.S., A.E.L., E.M., M.P.K., A.B.D.S. and K.A.K. prepared figures. A.B.D.S., A.E.L., M.P.K. and K.A.K. wrote the paper, and all authors provided critical feedback on early drafts. All authors read and approved the final manuscript.

Acknowledgements:

Coordenação de Aperfeiçoamento de Pessoal de Nível Superior (CAPES), Brazil for funding support to Ph.D Grant to Altair Brito dos Santos.

Dr. Arsenios Vlassis for contributions to the experimental design of imaging of cell lifetime.

The Lundbeck Foundation Initiative BRAINSTRUC (2015-2666) for funding support of L.K.S and A.E.L.

7 References

1. Abbott RD, Ross GW, White LR, Tanner CM, Masaki KH, Nelson JS, et al. Excessive daytime sleepiness and subsequent development of Parkinson disease. Neurology 2005; 65: 1442–6.
2. Angelova PR, Ludtmann MHR, Horrocks MH, Negoda A, Cremades N, Klenerman D, et al. Ca 2+ is a key factor in α-synuclein-induced neurotoxicity. J Cell Sci 2016; 129: 1792–801.
3. Barber TR, Lawton M, Rolinski M, Evetts S, Baig F, Ruffmann C, et al. Prodromal Parkinsonism and Neurodegenerative Risk Stratification in REM Sleep Behavior Disorder [Internet]. Sleep 2017; 40. Available from: https://academic.oup.com/sleep/article/doi/10.1093/sleep/zsx071/3796343
4. Bengoa-Vergniory N, Roberts RF, Wade-Martins R, Alegre-Abarrategui J. Alpha-synuclein oligomers: a new hope. Acta Neuropathol 2017; 134: 819–38.
5. Betzer C, Lassen LB, Olsen A, Kofoed RH, Reimer L, Gregersen E, et al. Alpha-synuclein aggregates activate calcium pump SERCA leading to calcium dysregulation. EMBO Rep 2018; 19: e44617.
6. Blythe SN, Wokosin D, Atherton JF, Bevan MD. Cellular Mechanisms Underlying Burst Firing in Substantia Nigra Dopamine Neurons. J Neurosci 2009; 29: 15531–41.
7. Boeve BF, Dickson DW, Olson EJ, Shepard JW, Silber MH, Ferman TJ, et al. Insights into REM sleep behavior disorder pathophysiology in brainstem-predominant Lewy body disease. Sleep Med 2007; 8: 60–4.
8. Boeve BF, Silber MH, Saper CB, Ferman TJ, Dickson DW, Parisi JE, et al. Pathophysiology of REM sleep behaviour disorder and relevance to neurodegenerative disease. Brain 2007; 130: 2770–88.
9. Boucetta S, Cisse Y, Mainville L, Morales M, Jones BE. Discharge Profiles across the Sleep-Waking Cycle of Identified Cholinergic, GABAergic, and Glutamatergic Neurons in the Pontomesencephalic Tegmentum of the Rat. J Neurosci 2014; 34: 4708–27.

10. Braak H, Ghebremedhin E, Rüb U, Bratzke H, Del Tredici K. Stages in the development of Parkinson's disease-related pathology. Cell Tissue Res 2004; 318: 121–34.
11. Buell AK, Dhulesia A, Mossuto MF, Cremades N, Kumita JR, Dumoulin M, et al. Population of Nonnative States of Lysozyme Variants Drives Amyloid Fibril Formation. J Am Chem Soc 2011; 133: 7737–43.
12. Coelho-Cerqueira E, Carmo-Gonçalves P, Sá Pinheiro A, Cortines J, Follmer C. α-Synuclein as an intrinsically disordered monomer - fact or artefact? FEBS J 2013; 280: 4915–27.
13. van Dort CJ, Zachs DP, Kenny JD, Zheng S, Goldblum RR, Gelwan N a, et al. Optogenetic activation of cholinergic neurons in the PPT or LDT induces REM sleep. Proc Natl Acad Sci 2015; 112: 584–9.
14. Fink AL. The Aggregation and Fibrillation of α-Synuclein. Acc Chem Res 2006; 39: 628–34.
15. Geng X, Lou H, Wang J, Li L, Swanson AL, Sun M, et al. α-Synuclein binds the K ATP channel at insulin-secretory granules and inhibits insulin secretion. Am J Physiol Metab 2011; 300: E276–86.
16. Ipsen TH, Polli FS, Kohlmeier KA. Calcium rises induced by AMPA and nicotine receptors in the ventral tegmental area show differences in mouse brain slices prenatally exposed to nicotine. Dev Neurobiol 2018; 78: 828–48.
17. Kroeger D, Ferrari LL, Petit G, Mahoney CE, Fuller PM, Arrigoni E, et al. Cholinergic, Glutamatergic, and GABAergic Neurons of the Pedunculopontine Tegmental Nucleus Have Distinct Effects on Sleep/Wake Behavior in Mice. J Neurosci 2017; 37: 1352–66.
18. Leng Y, Goldman SM, Cawthon PM, Stone KL, Ancoli-Israel S, Yaffe K. Excessive daytime sleepiness, objective napping and 11-year risk of Parkinson's disease in older men. Int J Epidemiol 2018; 47: 1679–86.
19. van Maarschalkerweerd A, Vetri V, Langkilde AE, Foderà V, Vestergaard B. Protein/Lipid Coaggregates are Formed During α-Synuclein-Induced Disruption of Lipid Bilayers. Biomacromolecules 2014; 15: 3643–54.
20. Michel PP, Toulorge D, Guerreiro S, Hirsch EC. Specific needs of dopamine neurons for stimulation in order to survive: implication for Parkinson disease. FASEB J 2013; 27: 3414–23.
21. Mironov SL. α-Synuclein forms non-selective cation channels and stimulates ATP-sensitive potassium channels in hippocampal neurons. J Physiol 2015; 593: 145–59.
22. Müller MLTM, Bohnen NI. Cholinergic Dysfunction in Parkinson's Disease. Curr Neurol Neurosci Rep 2013; 13: 377.
23. Postuma RB, Gagnon J-F, Bertrand J-A, Genier Marchand D, Montplaisir JY. Parkinson risk in idiopathic REM sleep behavior disorder: Preparing for neuroprotective trials. Neurology 2015; 84: 1104–13.
24. Postuma RB, Iranzo A, Hu M, Högl B, Boeve BF, Manni R, et al. Risk and predictors of dementia and parkinsonism in idiopathic REM sleep behaviour disorder: a multicentre study. Brain 2019; 142: 744–59.

25. Schenck CH, Bundlie SR, Mahowald MW. Delayed emergence of a parkinsonian disorder in 38% of 29 older, men initially diagnosed with idiopathic rapid eye movement sleep behavior disorder. Neurology 1996; 46: 388–93.
26. Schenck CH, Mahowald MW. REM sleep behavior disorder: Clinical, developmental, and neuroscience perspectives 16 years after its formal identification in SLEEP. Sleep 2002; 25: 120–38.
27. Uchiyama M, Isse K, Tanaka K, Yokota N, Hamamoto M, Aida S, et al. Incidental Lewy body disease in a patient with REM sleep behavior disorder. Neurology 1995; 45: 709–12.
28. Veleanu M, Axen TE, Kristensen MP, Kohlmeier KA. Comparison of bNOS and ChAT immunohistochemistry in the Laterodorsal Tegmentum (LDT) and the Pedunculopontine Tegmentum (PPT) of the mouse from brain slices prepared for electrophysiology. J Neurosci Methods 2016; 263: 23–35.
29. Wang Y, Shi M, Chung KA, Zabetian CP, Leverenz JB, Berg D, et al. Phosphorylated alpha-Synuclein in Parkinson's Disease. Sci Transl Med 2012; 4: 121ra20-121ra20.

Figures

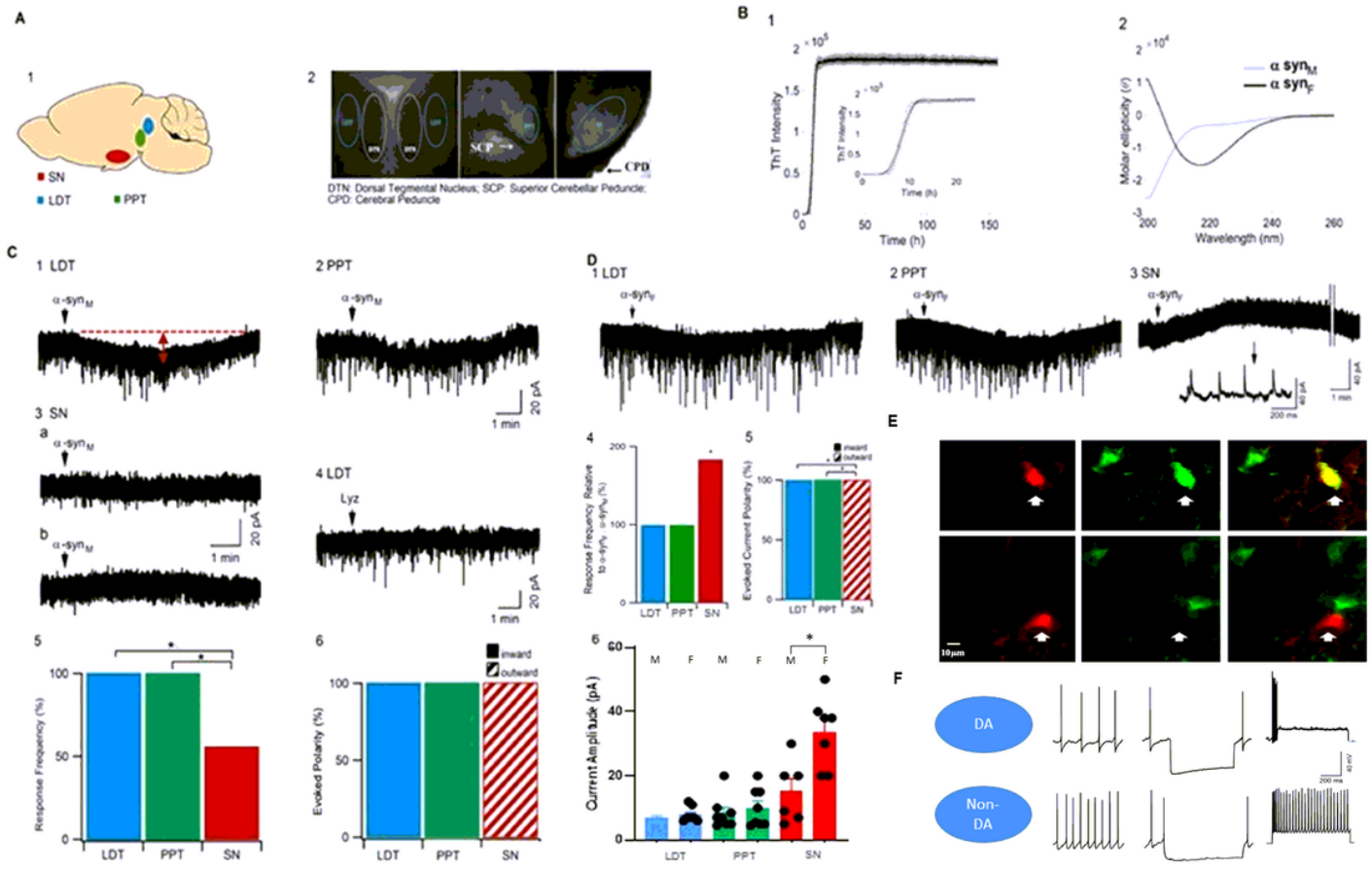

Figure 1

Monomeric α-syn induced contrasting current changes in neurons in sleep and motor control nuclei. (A1) The LDT, PPT and SN are shown in a mouse brain sagital view. (A2) Boundaries of the recorded nuclei along with other rostro-caudal extent-marking anatomical structures can be seen. B) α-syn fibrillation and characterization. C) Sample membrane responses to monomeric α-syn, which induced excitatory currents in LDT (C1) and PPT (C2) neurons. In contrast, in both putatively dopamine and non-dopaminergic SN neurons monomeric α-syn induced no response (C3a) or an inhibitory current (C3b). Lysozyme (Lyz) failed to elicit a membrane response (C4). The proportion of cells responding to, (C5) and the polarity of the current evoked (C6) by, monomeric α-syn differed markedly between the sleep-related and SN nuclei. D) The fibril form of α-syn induced disparate currents in sleep-related and motor control nuclei. Fibril α-syn elicited inward currents in LDT (D1) and PPT neurons (D2), but outward currents in SN neurons (D3). The proportion of SN cells responding to fibril was significantly higher than to monomeric α-syn (D4). (D5) A significant difference in the current amplitude elicited in SN neurons by the two α-syn forms was present. Such difference was not seen in either LDT or PPT cells (D6). In this panel, M indicates monomeric α-syn and F indicates the fibril form. E) bNOS immunohistochemistry revealed monomeric and fibril forms of α-syn induced inward currents in both cholinergic and non-cholinergic LDT cells. Both cells in E responded with inward currents. The cell in the top was cholinergic (bNOS-positive); whereas the cell in the bottom was negative. F) Representative examples of current clamp recordings of 2 types of responding SN neurons which were differentiated by their electrophysiological signatures. In this, and subsequent figures, '*' and '**' indicates $p < 0.05$ and $p < 0.01$, respectively.

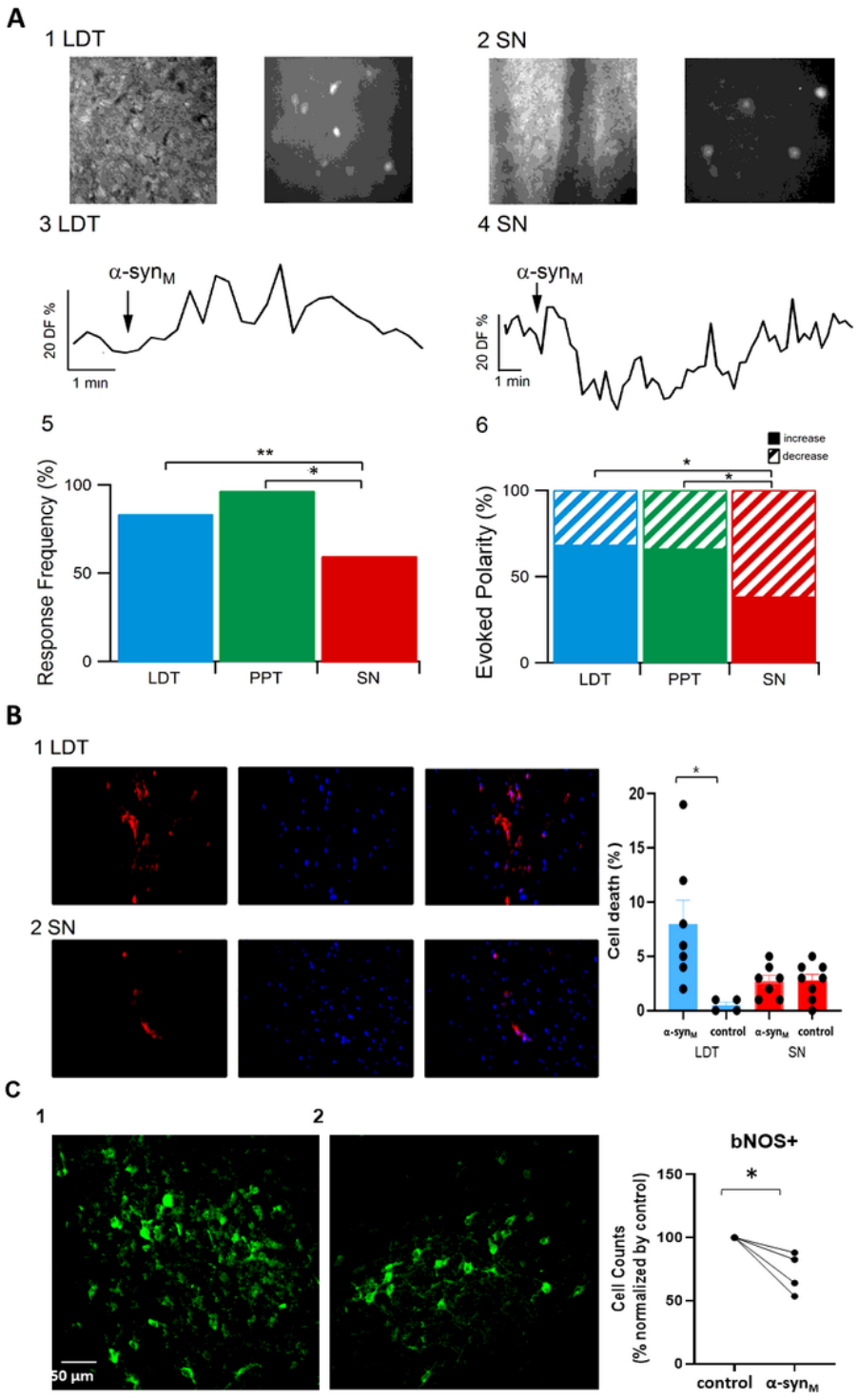

Figure 2

A) Representative image under bright field illumination and under fluorescence of fura-2 loaded neurons within LDT (A1) and SN (A2). Sample effects of monomeric α-syn on fluorescence indicative of alterations in intracellular calcium levels in LDT (A3) and SN (A4) cells. Summary data from the population of recorded cells showed that the proportion of cells responding to monomeric α-syn (A5), and the valence of calcium effects (A6) differed significantly between the sleep-related nuclei and SN. α-synM

indicates monomeric forms of the protein. B) Monomeric α-syn selectively facilitated cell death. Fluorescent images of LDT (B1) and SN brain slices (B2) exposed to monomeric α-syn showing dead cells in red (PI-positive, left) and live cells in blue (DAPI-positive, middle) with the two fields overlaid (right). As shown in the bar graphs to the right, there was a significantly greater percentage of cell death over control in the population of LDT cells exposed to monomeric α-syn, whereas in the SN, cell death was not significantly different between control and α-syn-exposed slices. C) Quantification of bNOS-positive cells in bisected slices revealed a smaller number of cholinergic neurons within α-synM-exposed half slices (C2) when compared to the number in the equivalent region in the other half of the slice incubated in control solution (C1) for the same time period. (C1, 2). A count of bNOS-positive cells revealed 14.7% fewer cholinergic cells in the α-synM-incubated, hemi-slices (200 nM; n=2) relative to control, and 47.3% fewer when incubated in 500 nM (n=2), which constituted a significant difference (Paired Student's t-test; df: 6; $p = 0.04$ * indicates $p < 0.05$). These data are consistent with current hypotheses regarding the role played by pontine cholinergic dysfunction in prodromal, or early-appearing, non-motor symptoms of PD (Müller and Bohnen, 2013).

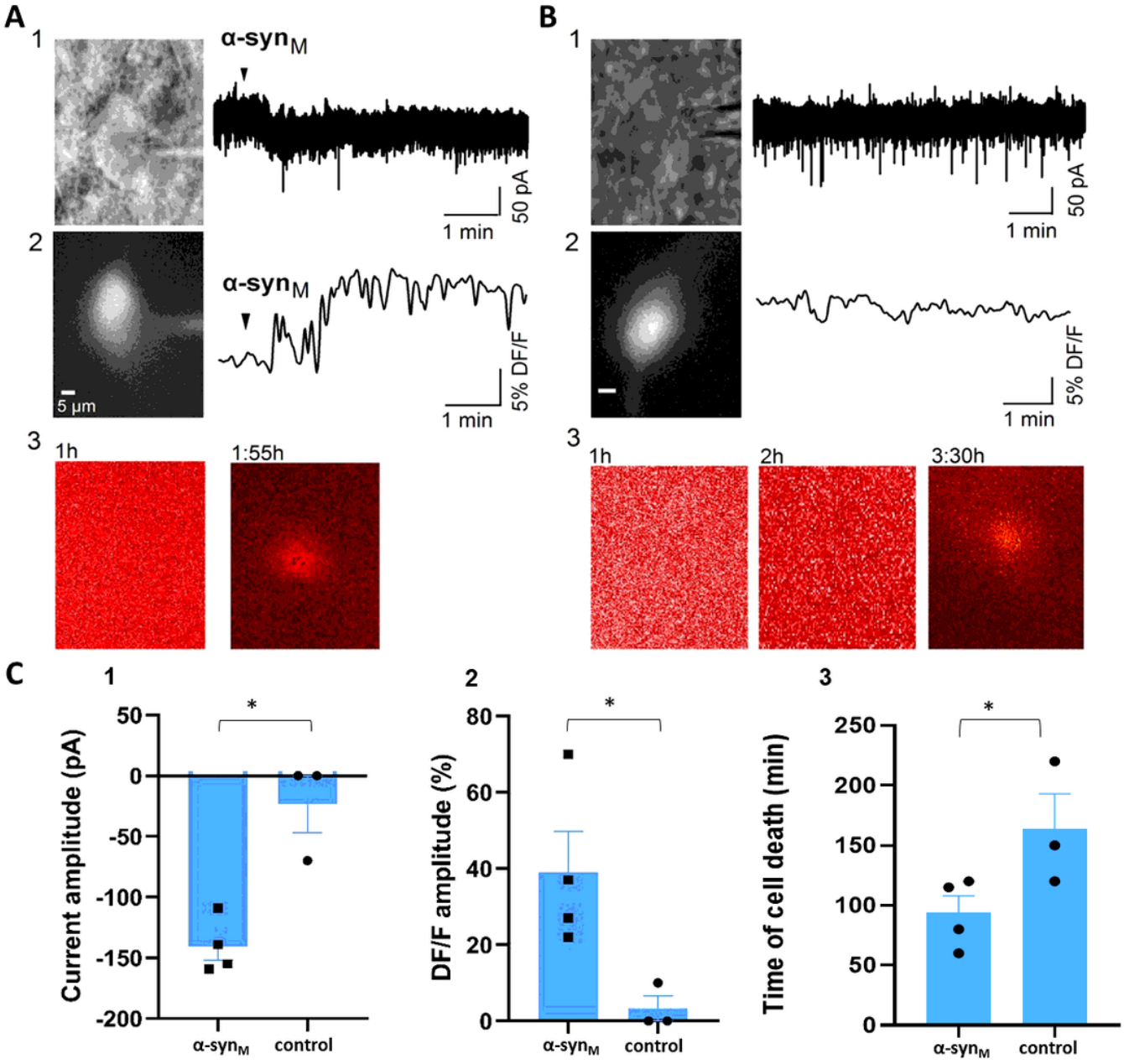

Figure 3

Real-time recordings of cell death were conducted in LDT neurons from which membrane responses and calcium rises were induced by α-syn. A) Representative example of the responses of a LDT neuron, which is shown in bright field in (A1), and in fluorescence in (A2), to application of monomeric α-syn. As can be seen, patch clamp recordings revealed induction of an inward membrane current (A1), and fluorescence changes indicative of an increase in intracellular calcium concentration (A2) following application of α-syn. Real-time visualization of the PI fluorescence signal in the same cell revealed cell death at 1:55 h following α-syn exposure (A3). B) Similar recordings were conducted in LDT neurons in control conditions, as illustrated by this example of a patch clamp recorded cell shown under bright field (B1),

and under fluorescent optics in (B2). Control solution did not elicit any changes in membrane current or intracellular calcium. However, it should be noted that in control conditions, when the perfusion was halted, we observed a change in the membrane current in one recorded cell suggesting mechanical disturbance. Live cell imaging from this cell showed that cell death occurred at 3:30 h (B3). C) Analysis showed that the same population of LDT cells which exhibited significantly different α-syn-mediated inward currents (Unpaired Student's t-test, $t(5) = 4.94$, $p = 0.004$) (C1) and rises in fluorescence (Unpaired Student's t-test, $t(5) = 2.78$, $p = 0.04$) (C2) from control also demonstrated significantly shorter cell lifetimes compared to control LDT neurons to which α-syn was not applied (C3).

Supplementary Files

This is a list of supplementary files associated with this preprint. Click to download.

- SupplementarymaterialMolecularNeurodegeneration.docx